International Journal of Fatigue 80 (2015) 136–144

Contents lists available at ScienceDirect

International Journal of Fatigue

journal homepage: www.elsevier.com/locate/ijfatigue

An energy method for rapid evaluation of high-cycle fatigue parameters based on intrinsic dissipation

Qiang Guo [a], Xinglin Guo [a,*], Junling Fan [b], Rizwanulhaque Syed [c], Chengwei Wu [a]

[a] State Key Laboratory of Structural Analysis for Industrial Equipment, Department of Engineering Mechanics, Dalian University of Technology, Dalian 116024, China
[b] Aircraft Strength Research Institute, Xi'an 710065, China
[c] Department of Mechanical Engineering, Dalian University of Technology, Dalian 116024, China

ARTICLE INFO

Article history:
Received 7 April 2015
Accepted 27 April 2015
Available online 14 May 2015

Keywords:
High-cycle fatigue
Intrinsic dissipation
Temperature variation
Damage mechanism

ABSTRACT

The present paper, firstly, establishes a calculation model of intrinsic dissipation, based on the double exponential regression for the one-dimensional distribution of specimen surface temperature variation. Then, an energy method is proposed for rapid evaluation of high-cycle fatigue parameters (i.e., fatigue limit and *S–N* curve). The energy method takes intrinsic dissipation as the fatigue damage indicator, and eliminates the interference of internal friction causing no damage on fatigue life evaluation. An experimental research on FV520B stainless steel was performed, in order to verify the feasibility and validity of the energy method, as well as the calculation model.

1. Introduction

High-cycle fatigue is one of the main failure modes occurring in engineering materials and mechanical components. Evaluation of high-cycle fatigue parameters (i.e., fatigue limit and *S–N* curve) is of significant importance to industrial production and scientific research. Since the traditional experimental method is time-consuming and costly, many alternative approaches have been developed to rapidly evaluate high-cycle fatigue parameters. As we all know, fatigue damage evolution is an energy dissipation process accompanied with temperature variation. Thus, most of those approaches are based on the analysis of the correlation between fatigue damage and corresponding temperature signal, such as one curve method [1], two curves method [2,3] and temperature integral method [4]. However, temperature variation under fatigue load is not an intrinsic manifestation uncovering material microstructure evolution, because it is affected by the internal thermal conduction and the thermal exchanges with ambient environments. Therefore, some researchers have started to develop new methods by reconstructing heat sources from temperature fields and taking dissipated energy as a fatigue damage indicator due to its clearer physical meaning and higher sensitivity to microstructure evolution.

Meneghetti et al. [5–8] developed a theoretical model to derive specific heat loss per cycle from temperature measurements performed. They proved that the specific heat loss is dependent on the applied stress amplitude and load ratio. In other words, it is irrelevant to the loading modes (stress-controlled or strain-controlled) and the specimen geometry (plain or notched). Chrysochoos et al. [9–11] developed a local heat diffusion equation to separately estimate the coupling sources and the dissipative sources for fatigue process analysis. An infrared image processing procedure was proposed to implement this estimation. Maquin et al. [12–14] developed an experimental method and a data processing procedure to obtain the small heat source generated during the very first cycles and to reveal the physical basis of the rapid determination of fatigue limit. Yang et al. [15,16] established the one-dimensional distribution of specimen surface temperature and determined the fatigue life using local plastic work. In addition, Delpueyo et al. [17] demonstrated a post-processing technique of infrared thermography images based on a derivative Gaussian filter to reconstruct heat source fields.

Inspired by those previous studies, this paper proposed a new calculation model of intrinsic dissipation and an energy method for rapid evaluation of high-cycle fatigue parameters (Section 2). In order to demonstrate the feasibility and validity, an experimental research on the fatigue behavior of FV520B stainless steel was performed (Section 3). The experimental results are analyzed and discussed (Section 4) before drawing some valuable conclusions (Section 5). As for the applicability of the energy method for other materials, we will further perform more experiments to study.

* Corresponding author. Tel./fax: +86 411 84707542.
E-mail address: xlguo@dlut.edu.cn (X. Guo).

http://dx.doi.org/10.1016/j.ijfatigue.2015.04.016
0142-1123/

2. Theoretical framework

2.1. A computation model of intrinsic dissipation

Fatigue damage is an irreversible thermodynamic process accompanied by energy dissipation. Most of the dissipated energy is converted into heat inducing temperature change. Many experiments have indicated that the surface temperature of a specimen or a component, subjected to fatigue load above its fatigue limit and below its yield limit, is well defined by three phases, including (I) initial temperature increase phase, (II) temperature stabilization phase, and (III) abrupt temperature increase phase before fatigue failure [18], as shown in Fig. 1. Among these three phases, phase II occupies almost 90% of the whole fatigue life for many metal materials, such as some iron–carbon alloys [19]. Thus, the temperature signal of this phase is widely applied to the evaluation of fatigue parameters.

For a flat and thin specimen, the measured surface temperature map is assumed to be very close to the depthwise averaged temperature field. Then combining the first and second laws of thermodynamics and neglecting the coupling effect between internal variables and temperature, the one-dimensional state equation of the specimen during the fatigue process can be written as [9,10]:

$$\rho C\left(\frac{\partial\theta(x,t)}{\partial t}+\frac{\theta(x,t)}{\tau_{\text{th}}^{\text{1D}}}\right)-k\frac{\partial^2\theta(x,t)}{\partial x^2}=s_{\text{the}}(t)+d_1(t) \tag{1}$$

where θ stands for the temperature variation, s_{the} denotes the thermoelastic source, d_1 signifies the intrinsic dissipation source (also called mechanical dissipation source), and ρ, C and k represent the material thermodynamic parameters: the mass density, the specific heat and the heat conduction coefficient, respectively. The symbol $\tau_{\text{th}}^{\text{1D}}$ stands for a time constant characterizing the lateral heat exchanges (i.e., thermal convection and radiation) between the specimen surface and the surroundings. Before the onset of damage localization, the thermoelastic source and the intrinsic dissipation source, just like stress and strain fields, are uniform within the specimen gauge part with constant cross-section at a macroscopic scale of observation [12,13].

Only high-cycle fatigue with sinusoidal load is considered in this study. For each load cycle, averaging Eq. (1) in the time domain (from t_i to $t_i + 1/f_{\text{L}}$, f_{L} and t_i being the loading frequency and the start time of the load cycle, respectively) leads to the following form:

$$\rho C\left(\hat{\theta}+\frac{\bar{\theta}(x,i)}{\tau_{\text{th}}^{\text{1D}}}\right)-k\frac{\partial^2\bar{\theta}(x,i)}{\partial x^2}=\bar{s}_{\text{the}}(i)+\bar{d}_1(i) \tag{2}$$

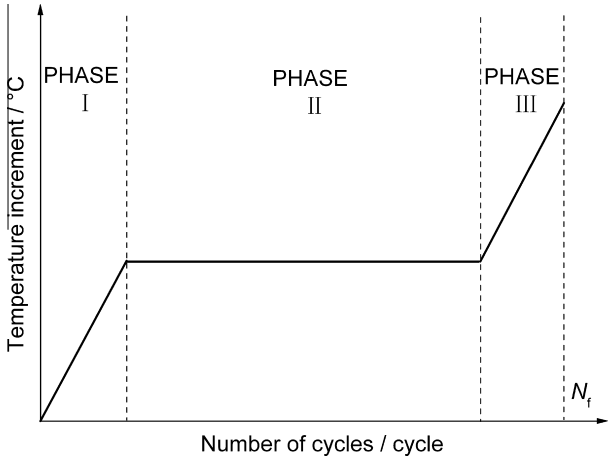

Fig. 1. Typical temperature evolution during fatigue test.

where

$$\begin{cases}\bar{d}_1(i)=f_{\text{L}}\int_{t_i}^{t_i+1/f_{\text{L}}} d_1(\tau)d\tau\\ \bar{s}_{\text{the}}(i)=f_{\text{L}}\int_{t_i}^{t_i+1/f_{\text{L}}} s_{\text{the}}(\tau)d\tau\\ \bar{\theta}(x,i)=f_{\text{L}}\int_{t_i}^{t_i+1/f_{\text{L}}} \theta(x,\tau)d\tau\\ \hat{\theta}(x,i)=f_{\text{L}}\int_{t_i}^{t_i+1/f_{\text{L}}} \frac{\partial\theta(x,\tau)}{\partial\tau}d\tau\end{cases} \tag{3}$$

Among them, $\bar{d}_1$ is the focus of particular concern denoting the average time rate of the intrinsic dissipation source during one load cycle, and its unit of measure is the same as that of d_1 (i.e. $\text{J m}^{-3}\,\text{s}^{-1}$). For the specimen in the temperature stabilization phase, both the accumulations of the thermoelastic source and the temperature change rate become zero at the end of every complete load cycle:

$$\begin{cases}\int_{t_i}^{t_i+1/f_{\text{L}}} s_{\text{the}}(\tau)d\tau=0\\ \int_{t_i}^{t_i+1/f_{\text{L}}} \frac{\partial\theta(x,\tau)}{\partial\tau}d\tau=0\end{cases} \tag{4}$$

Consequently, Eq. (2) can be simplified as:

$$\rho C\frac{\bar{\theta}(x,i)}{\tau_{\text{th}}^{\text{1D}}}-k\frac{\partial^2\bar{\theta}(x,i)}{\partial x^2}=\bar{d}_1(i) \tag{5}$$

For any given load cycle, Eq. (5) is actually a second-order linear differential equation with constant coefficients about spatial coordinate x. Mathematically, solving it leads to the following expression of general solution:

$$\bar{\theta}(x,i)=P_1\exp\left(x\sqrt{\frac{\rho C}{k\tau_{\text{th}}^{\text{1D}}}}\right)+P_2\exp\left(-x\sqrt{\frac{\rho C}{k\tau_{\text{th}}^{\text{1D}}}}\right)+\frac{\tau_{\text{th}}^{\text{1D}}\bar{d}_1(i)}{\rho C} \tag{6}$$

where P_1 and P_2 are arbitrary constants. Note from Eq. (6) that the distribution of the average temperature variation per load cycle, $\bar{\theta}(x,i)$, has the following double exponential function form within the specimen gauge part:

$$\bar{\theta}(x,i)=C_1(i)e^{rx}+C_2(i)e^{-rx}+C_3(i) \tag{7}$$

where C_1 and C_2 are the coefficients determined by the temperature boundary conditions, $r=\sqrt{\frac{\rho C}{k\tau_{\text{th}}^{\text{1D}}}}$ the parameter determined by the lateral heat exchanges with the surroundings, and $C_3(i)=\frac{\tau_{\text{th}}^{\text{1D}}\bar{d}_1(i)}{\rho C}$ the coefficient jointly determined by both the lateral heat exchanges and the intrinsic dissipation. As a consequence, the intrinsic dissipation rate per load cycle can be expressed as:

$$\bar{d}_1(i)=kr^2C_3(i) \tag{8}$$

where k is the heat conduction coefficient of material as defined above, r and $C_3(i)$ the parameters which can be determined in actual experiments by regressing the temperature data $\bar{\theta}(x,i)$ in according to its double exponential distribution model (i.e. Eq. (7)).

2.2. An energy method for fatigue evaluation

As a process of energy dissipation, fatigue damage involves in a nonlinear thermal–mechanical coupled effect caused by intrinsic dissipation. In fact, the essence of intrinsic dissipation is the energy form of the entropy generation contributed by non-heat-conduction factors in unit time [11,20,21]:

$$\begin{aligned}d_1&=T\left(\rho\dot{s}-\text{div}\left(\frac{k\,\text{grad}T}{T}\right)-\frac{k\,\text{grad}T}{T^2}\cdot\text{grad}T\right)=T(\eta-\eta_2)\\&=T\eta-d_2\end{aligned} \tag{9}$$

where T is the absolute temperature, s stands for the entropy density, $\eta=\rho\dot{s}-\text{div}\left(\frac{k\,\text{grad}T}{T}\right)$ denotes the rate of entropy generation,

and $\eta_2 = \frac{k\ \mathrm{grad}T}{T^2} \cdot \mathrm{grad}T$ represents the part of the entropy generation rate contributed by heat-conduction factors whose energy form, $d_2 = T\eta_2$, is referred to as thermal dissipation. According to the Clausius inequality, the entropy generation rate as a quantitative characterization of the irreversible process is always positive, and the intrinsic dissipation d_1 is as well. Generally speaking, almost all materials inevitably contain some defects, such as vacancies, dislocations and grain boundaries. This permits irreversible microstructure evolution to occur even under relatively low alternating stress, including dislocation intersection, multiplication, pile-up, etc. These irreversible changes of material microstructure, collectively referred to as microplastic deformation, inevitably lead to entropy generation manifested as intrinsic dissipation [22–24]. For this reason, intrinsic dissipation has relatively high sensitivity to microstructure evolution. It is precisely the material microplastic deformation that causes the fatigue damage and further results in the final fatigue failure. As a consequence, it is of great significance to use intrinsic dissipation as a fatigue damage indicator with definite physical meaning to evaluate high-cycle fatigue parameters. Nevertheless, we should note that intrinsic dissipation is induced not only by microplastic deformation (unrecoverable microstructure motion), but also by internal friction (recoverable microstructure motion) such as the oscillation of dislocation loops, which does not contribute to the material fatigue damage [12–14,25–28].

For the alternating stress below the fatigue limit, microplastic deformation can be considered negligible since the mechanical behavior of material is mainly related to recoverable microstructure motion. The intrinsic dissipation under such stress condition is almost completely caused by internal friction and the fatigue life is deemed infinite [12–14,27,28]. On the contrary, for the alternating stress above the fatigue limit, microplastic deformation appears and induces fatigue damage . In this case, the intrinsic dissipation actually includes two parts: one caused by internal friction, and the other one caused by microplatic deformation [12–14,27,28]. Moreover, the latter is generally more sensitive than the former to the increase of the alternating stress amplitude, which can be explained by that microplastic deformation directly and significantly increases the degree of disorder of material microstructure (i.e. the entropy of material) inducing violent intrinsic dissipation. As a conclusion, the fatigue limit of material actually corresponds to a critical value of stress amplitude, at which the generation mechanism of intrinsic dissipation transits from internal friction to the combined effect of internal friction and microplastic deformation.

On the basis of the above analysis and conclusion, an energy method for rapidly evaluating the fatigue limit is proposed, whose basic idea is to find the critical value of stress amplitude through analyzing the stress amplitude dependence of intrinsic dissipation. Specifically, implementation of this energy method relies on a successive stepped loading test performed with a flat and thin specimen made of the material. Through this test, we can readily obtain the stable temperature variations of the specimen under different alternating stress amplitudes by means of a full-field thermographic technique. And then the corresponding intrinsic dissipation rate per load cycle, $\tilde{d}_1(i)$, can be calculated using the calculation model introduced above. In order to reduce random errors, an arithmetic mean value of $\tilde{d}_1(i)$, corresponding to a certain number of successive complete load cycles, is also calculated:

$$\tilde{d}_1 = \frac{1}{n}\sum_{i=m}^{m+n-1}\tilde{d}_1(i) \tag{10}$$

where m represents the initial load cycle and n the sum of the load cycles used for averaging, n being 150 in present research. Inspired by the two curves method [2,3] and the corresponding iteration procedure [29], we utilize two straight lines to interpolate the experimental data pairs $(\sigma_{a_j}, \tilde{d}_{1_j})$ as illustrated in Fig. 2, one straight line for the stress amplitudes below the fatigue limit and the other one for those above it:

$$\begin{cases} \tilde{d}_{1_j} = a\sigma_{a_j} + b & (\sigma_{a_j} \leqslant \sigma_0) \\ \tilde{d}_{1_j} = A\sigma_{a_j} + B & (\sigma_{a_j} > \sigma_0) \end{cases} \tag{11}$$

where j is the index of the loading stages corresponding to different alternating stress amplitudes, and $\tilde{d}_{1_j}$ the intrinsic dissipation rate under the alternating stress amplitude σ_{a_j}. The intersection point of the two least-square fitting straight lines implies the transition of the generation mechanism of intrinsic dissipation. Correspondingly, the abscissa value of this point is just the critical value of stress amplitude that we seek, i.e., the fatigue limit.

According to the damage accumulation theory, fatigue failure is a result of the continual accumulation of fatigue damage [30,31]. The damage accumulation process related to irreversible microstructure evolution can be quantitatively described with the accumulation of intrinsic dissipation. Since the intrinsic dissipation under the alternating stress above the fatigue limit consists of two parts and only the part induced by microplastic deformation is associated with the fatigue damage, it is necessary to extract this part from the total intrinsic dissipation for accurately estimating damage. For this purpose, the following two hypotheses are put forward: the fitting straight line of the experimental data pairs $(\sigma_{a_j}, \tilde{d}_{1_j})$ below the fatigue limit can define a linear relationship between the stress amplitude and the other part of the intrinsic dissipation induced by internal friction, and this linear relationship is applicable for the ones above the fatigue limit, as illustrated in Fig. 2. Based on these two hypotheses and considering the overwhelming proportion of the temperature stabilization phase in the whole fatigue life, a threshold value representing fatigue failure, E_C, is determined by the follow expression:

$$E_C = \frac{N_f}{f_L}\left[\tilde{d}_1 - (a\sigma_a + b)\right] \quad (\sigma_a > \sigma_0) \tag{12}$$

where a and b are respectively the slope and the intercept of the fitting straight line below the fatigue limit, and $\tilde{d}_1$ and N_f are respectively the intrinsic dissipation rate and the fatigue life under the stress amplitude σ_a. It is worth noting that a and b have been identified in the stepped loading test, and that $\tilde{d}_1$ and N_f can be obtained by a constant amplitude fatigue test where the applied stress amplitude σ_a is an arbitrary reasonable value. The threshold value E_C is, in

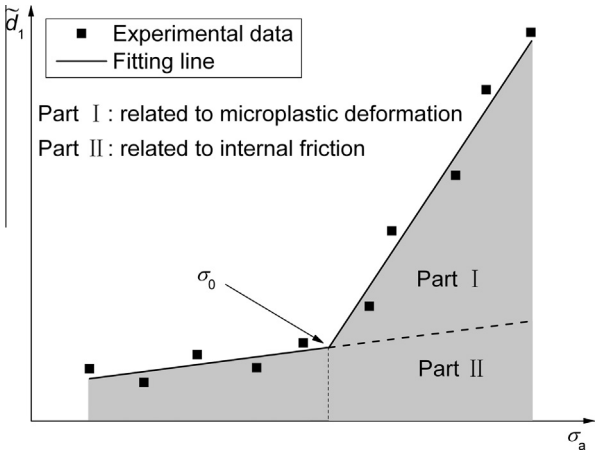

Fig. 2. The energy method for determining the fatigue limit and the part of the intrinsic dissipation induced by microplastic deformation.

fact, the cumulant of the part of the intrinsic dissipation induced by microplastic deformation over the whole fatigue life, and it is considered as a material constant independent of loading history. In other words, fatigue failure occurs once this part of the intrinsic dissipation accumulates to E_C, no matter what alternating stress the specimen is subjected to. Thus, the fatigue lives N_{f_j} under the different stress amplitudes σ_{a_j} are estimated by:

$$N_{f_j} = \frac{E_C f_L}{\tilde{d}_{1_j} - (a\sigma_{a_j} + b)} \quad (\sigma_{a_j} > \sigma_0) \tag{13}$$

Furthermore, the S–N curve of material can be plotted in bi-logarithm scale through fitting the data pairs (N_{f_j}, σ_{a_j}) by the least-square method.

3. Description of experiment

3.1. Material and specimen

The material investigated in the present research is a kind of precipitation-hardening martensite stainless steel FV520B, whose main chemical compositions are listed in Table 1. It is widely used for mechanical details with a much higher ultimate tensile strength of 1309 MP and a 0.2% offset yield strength of 1080 MPa after a series of specific heat treatments given in Table 2. Moreover, for calculating intrinsic dissipation, its heat conduction coefficient was experimentally measured to be $k = 15\ \mathrm{m^{-1}\ k^{-1}}$.

The fatigue test specimens were manufactured from a 5 mm thick plate of FV520B stainless steel with the length direction parallel to the rolling direction. Dimensions are shown in Fig. 3. All the specimens were polished with a sequence of emery papers to reduce the surface roughness induced by cutting. The effect of cutting process upon the material fatigue properties was therefore minimized. In order to eliminate the reflection from the external environment and to ensure the consistency of the surface emissivity, these specimens were evenly painted with a thin black coating with the emissivity coefficient equal to 0.95 or higher.

3.2. Experimental setup

The fatigue test machine was a fully computerized MTS810 servo-hydraulic system with a 100 kN capacity. The thermographic equipment was a Cedip Jade III infrared camera with a 320 × 240 pixels focal-plane-array InSb detector. Its spectrum response range is 3–5 μm, and the sensitivity/Noise Equivalent Temperature Difference (NETD) is less than 0.025 °C at 25 °C, generally 0.02 °C after a calibration operation which had been completed before this experiment. The infrared camera was kept in front of the specimen under test at a distance of 0.5 m, and hence its spatial resolution was as small as 157.9 μm.

In addition, for purpose of further reducing the influence of the external environment and improving the accuracy of the experiment, the lens of the infrared camera and the specimen under test were packed in a relatively closed space using a special thermal insulation material. The bottom grip connected to the actuator of the fatigue test machine was continuously cooled down by circulating water, so that the temperature boundary conditions of the specimen could always remain relatively stable during the whole fatigue testing.

Table 2
Heat treatments processes.

Type of heat treatment	Conditions	Holding time (h)
Solution treatment	1050 ± 10 °C, air-cooling	1.5–2.5
Thermal refining treatment	850 ± 10 °C, oil-cooling	1.5–2.5
Aging treatment	480 ± 10 °C, air-cooling	2.0–3.0

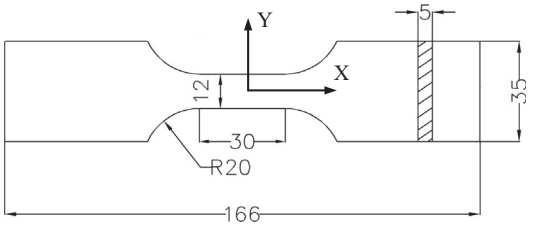

Fig. 3. Dimensions of the specimens (unit: mm).

3.3. Experimental procedure

Stress-controlled fatigue tests with a sinusoidal load were carried out on specimens at a loading frequency of $f_L = 10$ Hz and a stress ratio of $R = -1$ at normal room temperature. Thus the applied stress could be expressed as $\sigma(t) = \sigma_a \sin(20\pi t)$, σ_a being the alternating stress amplitude. The sampling frequency of the infrared camera was set to as high as $f_A = 150$ Hz, ensuring the accurate characterization of temperature variation. The whole procedure of the fatigue experiment included two parts, and every part used a new specimen without undergoing any loading.

The first part was a stepped loading test. The specimen was subjected to an alternating stress with the amplitude starting from 280 MPa to 440 MPa with a fixed step of 10 MPa per 10,000 load cycles, as shown in Fig. 4. The infrared camera recorded the temperature variation of the final successive 150 load cycles (i.e., 2250 infrared thermography images) for every loading stage. In these periods of time (i.e., 15 s before the end of every loading stage), the specimen surface temperature had already entered into the stabilization phase, only fluctuating periodically with the applied alternating stress.

The second part was a constant amplitude loading test. An alternating stress with the constant amplitude of 380 MPa was continuously applied to the specimen until the final fatigue failure occurred. The infrared camera recorded the final 150 load cycles of every 5000 load cycles.

4. Results and discussion

Fig. 5 shows the one-dimensional distribution of the average temperature variation of a certain load cycle under the stress amplitude of 360 MPa and its double exponential regression curve. Here we focus only on the middle segment of 22.90 mm in the specimen gauge part, which corresponds to 145 pixels of the infrared thermography image. It is, firstly, observed in Fig. 5 that the highest average temperature variation is not just located at the center of the specimen, in spite of the uniform distribution of heat sources at a macroscopic scale. This phenomenon is mainly due to the difference between the specimen's two ends in temperature

Table 1
Chemical compositions of FV520B steel (mass fraction/%).

C	Si	Mn	P	S	Ni	Cr	Cu	Nb	Mo
⩽0.07	⩽0.07	⩽1.0	⩽0.03	⩽0.03	5.0–6.0	13.2–14.5	1.3–1.8	0.25–0.45	1.3–1.8

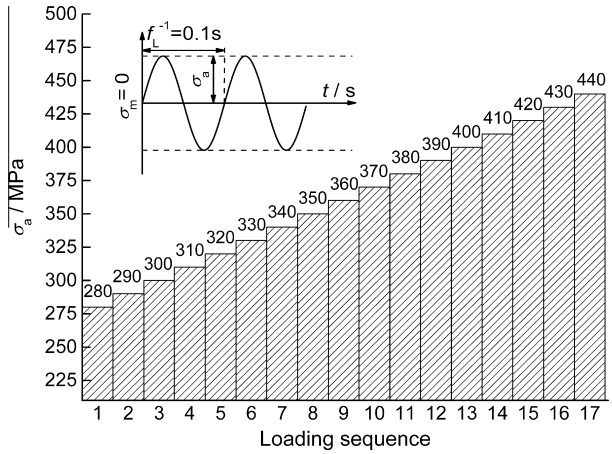

Fig. 4. Stepped loading procedure.

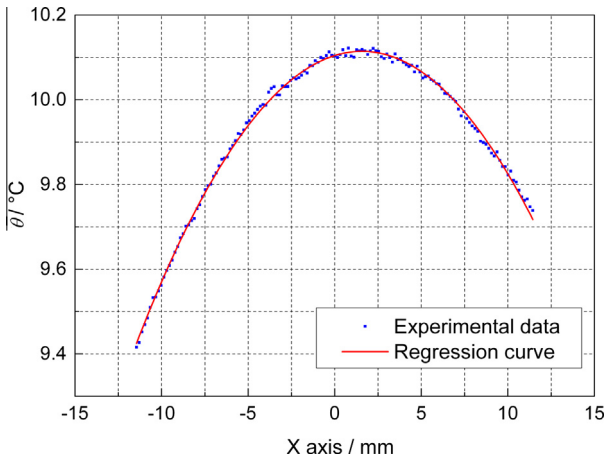

Fig. 5. One-dimensional distribution of the average temperature variation and its double exponential regression curve.

boundary conditions. In order to demonstrate the validity of the double exponential regression model (i.e., Eq. (7)), two statistical methods, namely, *F*-test and residual analysis [32,33], are adopted to analyze the regression effect. The coefficient of determination of *F*-test is as high as 0.9978 indicating that the regression model can perfectly explain the one-dimensional distribution of the temperature variation. Fig. 6 shows the distribution of the residuals and the statistic of the standard residuals. It can be recognized that almost all residual data points randomly distribute in a zonal region with the lines of the residuals equal to 0 °C, 0.02 °C and −0.02 °C as the centerline, the upper and lower boundaries, respectively. The residual limit of 0.02 °C is just the sensitivity of the infrared camera. Moreover, the statistical results of the standard residuals reveal that they basically obey normal distribution. Although here we only take a certain load cycle under the stress amplitude of 360 MPa as an example for illustrating the regression effect, it is true that the double exponential regression model is applicable for all temperature data acquired in the experiment and can achieve equally desirable regression effect.

Fig. 7 shows the regression curves of the average temperature variation under four different stress amplitudes respectively, indicating that the curvatures becomes higher and higher with the increase of the stress amplitude. The shapes of those regression curves intuitively character the intensities of intrinsic dissipation under their respective stress amplitudes. Generally speaking, on such non-adiabatic experimental conditions the higher the curvature of the regression curve, the higher the intrinsic dissipation rate. Making regression for all the acquired temperature data $\bar{\theta}$ in according to Eq. (7) and then performing calculation with the determined regression parameters by Eq. (8), we can obtain the intrinsic dissipation rates related to the final successive 150 load cycles of every loading stage, as shown in Fig. 8. It is clearly observed from the graph that for a given stress amplitude the intrinsic dissipation rate per load cycle has high stability, and between different stress amplitudes the intrinsic dissipation rates have significant difference increasing with the applied stress amplitude. Even so, we still adopt the arithmetic mean value of the final successive 150 load cycles per loading stage to characterize the corresponding intrinsic dissipation intensity for reducing the sampling errors as far as possible.

Fig. 9 illustrates the alternating stress amplitude dependence of the intrinsic dissipation rate, where the two lines are the least-square fitting straight lines of the experimental data pairs $(\sigma_{a_j}, \tilde{d}_{1_j})$ below and above the fatigue limit, respectively. The abscissa value of the intersection point is identified as the fatigue limit $\sigma_{0_{E1}} = 346.37$ MPa. Moreover, it is worth noting that the slopes of the two fitting lines are respectively 269.95 and 1867.15, with a significant difference of factor 5.91. Here we combine G-L dislocation model [34,35] and F-R dislocation multiplication theory [36,37] to reveal the material microstructure motion hidden behind this macroscopic phenomenon of energy dissipation. Within the material, there are a lot of dislocation lines. These dislocation lines, regarded as elastically vibrating strings, are fixed by pinning points in the crystal lattice. The pinning points fall into two categories, namely, the weak pinning points acted by solute atoms, vacancy defects, etc., and the strong pinning points acted by grain boundaries, secondary phase particles, etc. When the material is subjected to the stress amplitude below the fatigue limit, the dislocation lines gradually break away from the weak pinning points with the increase of the stress amplitude, and reversibly slide between the strong points [25,26]. The intrinsic dissipation due to this dislocation swing mechanism (i.e., internal friction effect) is proportional to the sweeping-over area of dislocation lines correlated positively with the applied stress in the material linear elasticity range. Therefore, the intrinsic dissipation rate has a good linear relationship with the applied stress amplitude. For the stress amplitudes above the fatigue limit, the dislocation lines break away from some strong pins. Meanwhile, some other strong pins, still unable to unpin, become dislocation sources generating new dislocation lines. The unpinning of strong pins and the dislocation multiplication can lead to permanent strain with irreversible microstructure evolution, namely, microplastic deformation [25,26]. As stated above, under such stress states one part of the intrinsic dissipation is related to the internal friction due to dislocation lines swing, while the other part is related to the microplastic deformation. And it is recognized from the experimental results that the latter is indeed more sensitive than the former to the increase of the applied stress amplitude. This is because the microplastic deformation, including the unpinning of strong pins and the dislocation multiplication, directly and significantly results in the increase of the disorder degree of material microstructure, and meanwhile, a large amount of energy is dissipated. From the perspective of physics, the critical value of stress amplitude, corresponding to the start of strong points unpinning or the start of dislocation multiplication, is a real sense of the fatigue limit.

Fig. 10 shows the evolution of the intrinsic dissipation rate under the stress amplitude of 380 MPa during the whole temperature stabilization phase. It is clearly observed that the intrinsic dissipation rate always remains relatively stable, indicating that the process of the material microstructure evolution is uniform during

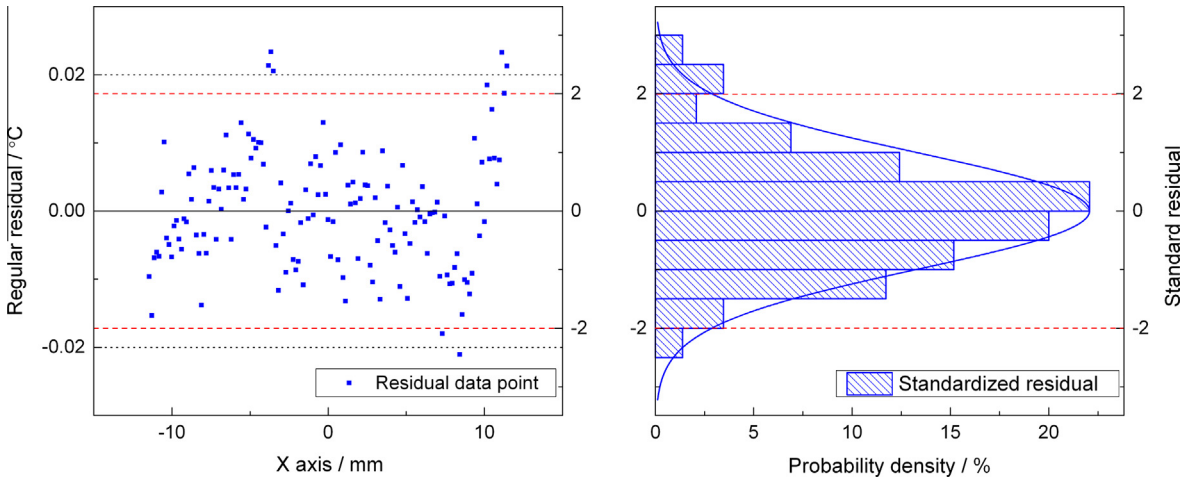

Fig. 6. Residual analysis plot of the double exponential regression.

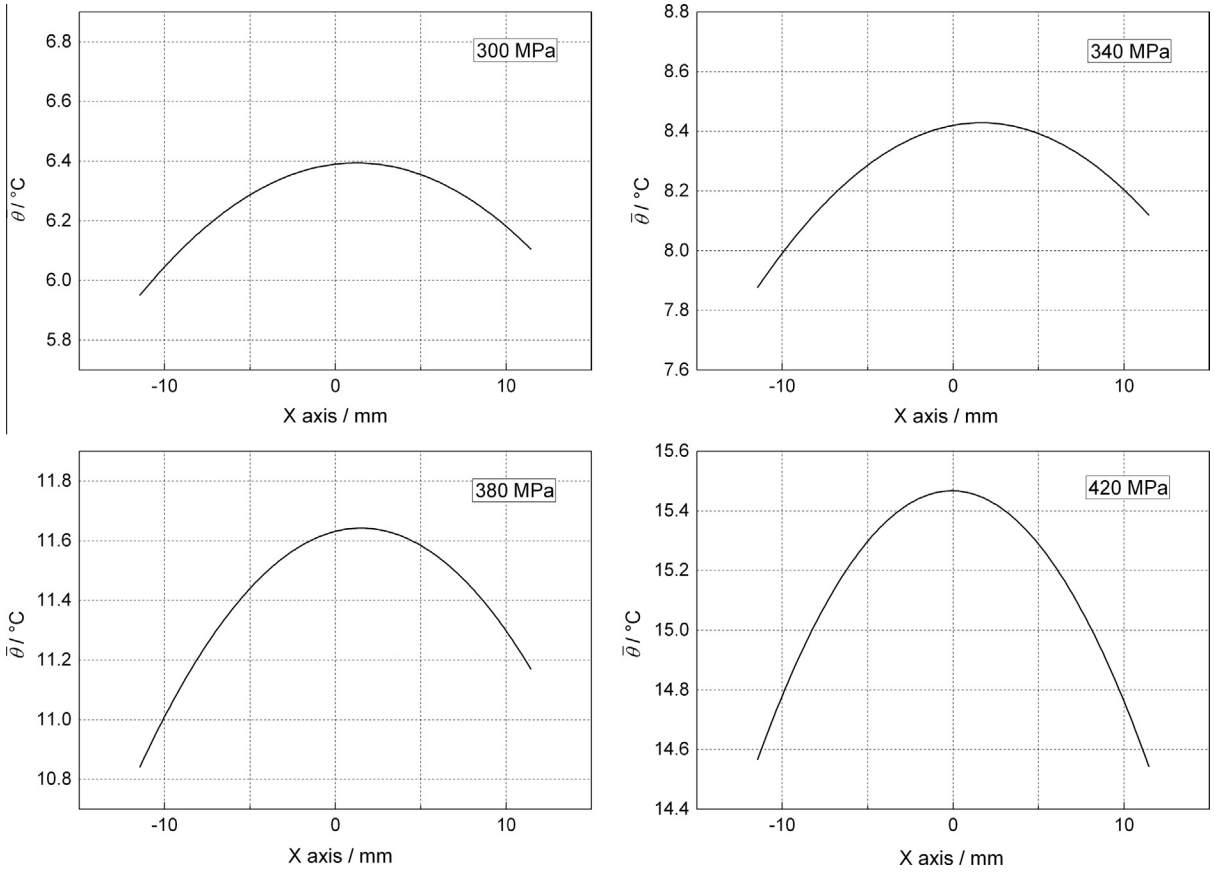

Fig. 7. Regression curves of average temperature variation under different stress amplitudes.

this phase. This is consistent with the theory of linear cumulative fatigue damage. In fact, it is just this favorable stability of the intrinsic dissipation rate that provides the possibility for only utilizing the arithmetic mean value of the final 150 load cycles per loading stage to characterize the intrinsic dissipation intensity under the corresponding stress amplitude. Making a simple calculation by Eq. (12), we can obtain the total accumulated quantity of the intrinsic dissipation caused by microplastic deformation in the whole fatigue life (388,327 load cycles), namely, the threshold value of fatigue failure $E_C = 1.7966 \times 10^9$ J m^{-3}. And then, the fatigue lives under different stress amplitudes can be easily calculated by Eq. (13).

Fig. 11 shows the S–N curves of different survival probabilities ($P_S = 50\%$ and $P_S = 97.7\%$) in bi-logarithm scale, by fitting the calculated data pairs (N_{f_j}, σ_{a_j}) with the least-square method and the log-normal distribution of fatigue lives [32,33]. The infinite fatigue life is defined as 10^6 cycles in this study, and accordingly the fatigue limit is evaluated as $\sigma_{0_{E2}} = 343.13$ MPa by extrapolating the S–N

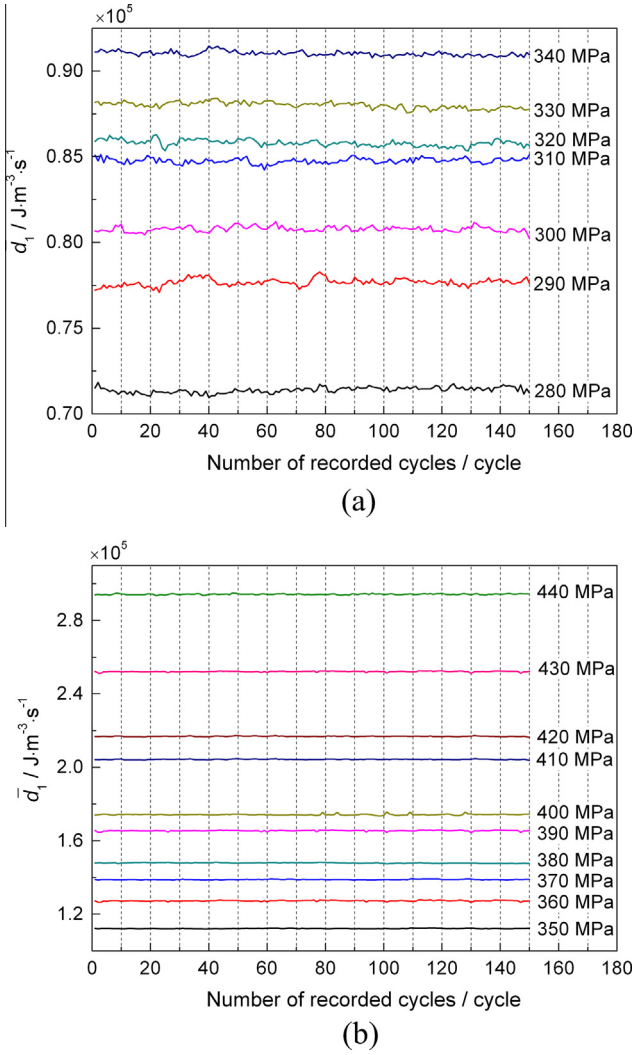

Fig. 8. Evolution of intrinsic dissipation rate during the final successive 150 load cycles of every loading stage: (a) below and (b) above the fatigue limt.

curve of $P_S = 50\%$ down to the specified cycle number 10^6. At the same time, the S–N curve at $P_S = 97.7\%$ is also calculated and plotted in Fig. 11 to meet the requirement of higher reliability in some special engineering domains. The corresponding fatigue limit is $\sigma_{0E2} = 333.02$ MPa. In addition, it is found that the higher the survival probability, the lower the fatigue strength and the fatigue limit.

In order to confirm the correctness and effectiveness of the energy method proposed, as well as the calculation model of intrinsic dissipation, the S–N curves obtained by the traditional testing method are presented in Fig. 12. The same bi-logarithm scale and the same data processing method are adopted for the sake of comparison. The fatigue limits σ_{0T} at $P_S = 50\%$ and $P_S = 97.7\%$ survival probabilities resorting to the traditional approach are determined as 339.56 MPa and 332.21 MPa, respectively. Table 3 presents the comparison results of the fatigue limits provided by the different methods. Percentage deviations $\delta\%$ are determined by the following formula:

$$\delta\% = \left|\frac{\Delta\sigma_{0T} - \Delta\sigma_{0E}}{\Delta\sigma_{0T}}\right| \times 100\% \tag{14}$$

Moreover, the slope and the intercept of the S–N curve of $P_S = 50\%$ survival probability predicted by the energy method are $K_E = -9.1333$ and $C_E = 29.1571$, separately. They are in good agreement with the ones obtained by the traditional method, namely, $K_T = -8.9382$ and $C_T = 28.6218$. Percentage deviations of K_E and C_E, with K_T and C_T as the references, are only 2.18% and 1.87%, respectively.

In summary, the energy method can achieve relatively high accuracy for evaluating the high-cycle fatigue parameters. Such high accuracy is attributed to three factors, namely, the accurate calculation of the intrinsic dissipation, the reasonable extraction of the part related to microplastic deformation, and the effective selection of the fatigue damage indicator. The proposed calculation model of intrinsic dissipation takes into consideration the full-field temperature within the specimen gauge part. This effectively reduces the random errors caused by only considering a certain local temperature. Among the whole intrinsic dissipation, only the part caused by irreversible microstructure evolution is associated with the fatigue life, because fatigue failure is considered as a result of the accumulation of microplastic deformation. Additionally, it should be underlined that the energy method, compared to the traditional approach, greatly shortens the experimental period and reduces the experimental cost.

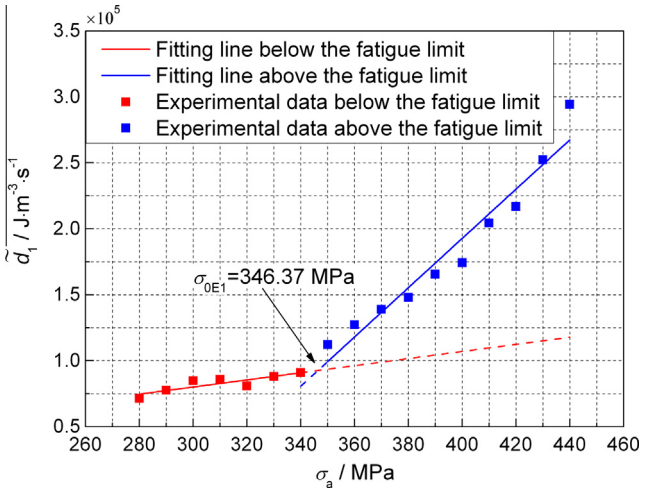

Fig. 9. The alternating stress amplitude dependence of the intrinsic dissipation rate and the fatigue limit $\sigma_{0_{E1}}$ obtained by the energy method.

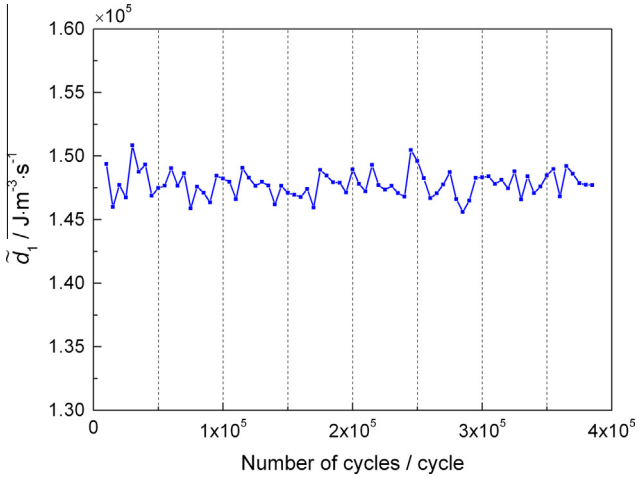

Fig. 10. The evolution of the average intrinsic dissipation rate under the stress amplitude of 380 MPa.

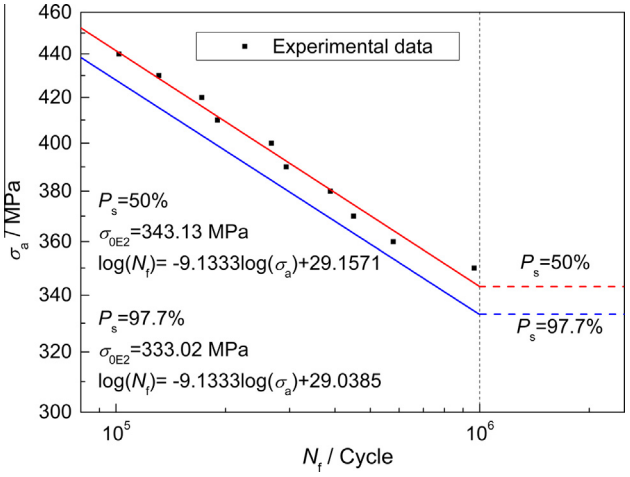

Fig. 11. *S–N* curves obtained by the energy method.

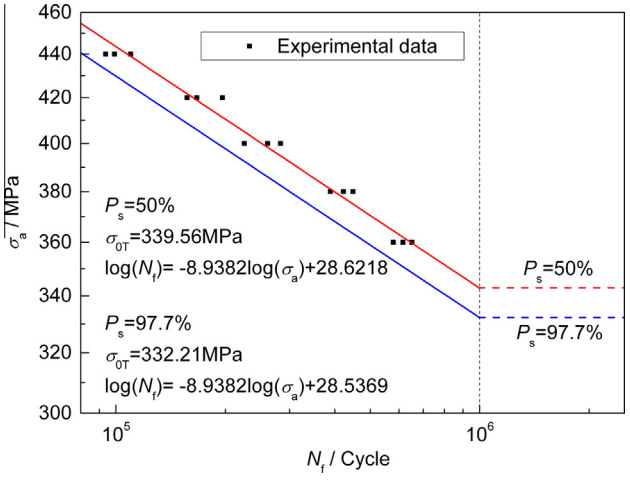

Fig. 12. *S–N* curves obtained by the traditional testing method.

Table 3
Comparison of the fatigue limits afforded by the different methods.

	Value (P_S = 50%) (MPa)	Error δ (%)	Value (P_S = 97.7%) (MPa)	Error δ (%)
σ_{0T}	339.56	–	332.21	–
σ_{0E1}	346.37	2.01		
σ_{0E2}	343.13	1.05	333.02	0.24

5. Conclusions

The present paper, firstly, establishes a calculation model of intrinsic dissipation, based on the double exponential regression for the one-dimensional distribution of specimen surface temperature variation. Then, an energy method is proposed to rapidly evaluate high-cycle fatigue parameters. This energy method takes intrinsic dissipation as the fatigue damage indicator, and eliminates the interference of internal friction causing no damage on fatigue life evaluation. Therefore, it can achieve relatively high prediction accuracy.

The analysis of the experimental results of FV520B stainless steel indicates that there is a critical value of stress amplitude at which the generation mechanism of intrinsic dissipation transits from internal friction to the combined effect of internal friction and microplastic deformation, namely, once the applied stress amplitude exceeds this critical value the strong points unpinning or the dislocation multiplication starts. Thus, this critical value of stress amplitude is the fatigue limit in a real sense. Moreover, the analysis indicates that the high-cycle fatigue process under a constant stress amplitude is a process with stable microstructure evolution characterized by a stable intrinsic dissipation rate. Fatigue failure occurs once the part of the intrinsic dissipation due to microplastic deformation accumulates to a threshold value E_C, which is a material constant independent of loading history.

Obviously, the main target of the present paper is to demonstrate the energy method for rapid evaluation of high-cycle fatigue parameters, as well as the calculation model of intrinsic dissipation. It can be inferred that they have a tremendous potential of application in the fields of the mechanism study on fatigue damage and the rapid evaluation of fatigue parameters.

Acknowledgements

We would like to thank the financial supports from Natural Science Foundation of China (No. 11072045) and National Basic Research Program of China (No. 2011CB706504).

References

[1] La Rosa G, Risitano A. Thermographic methodology for rapid determination of the fatigue limit of materials and mechanical components. Int J Fatigue 2000;22:65–73.
[2] Luong MP. Infrared thermographic scanning of fatigue in metals. Nucl Eng Des 1995;158:363–76.
[3] Luong MP. Fatigue limit evaluation of metals using an infrared thermographic technique. Mech Mater 1998;28:155–63.
[4] Fargione G, Geraci A, La Rosa G, Risitano A. Rapid determination of the fatigue curve by the thermographic method. Int J Fatigue 2002;24:11–9.
[5] Meneghetti G. Analysis of the fatigue strength of a stainless steel based on the energy dissipation. Int J Fatigue 2007;29:81–94.
[6] Meneghetti G, Ricotta M. The use of the specific heat loss to analyse the low- and high-cycle fatigue behaviour of plain and notched specimens made of a stainless steel. Eng Fract Mech 2012;81:2–16.
[7] Meneghetti G, Ricotta M, Atzori B. A synthesis of the push-pull fatigue behaviour of plain and notched stainless steel specimens by using the specific heat loss. Fatigue Fract Eng Mater 2013;36:1306–22.
[8] Meneghetti G, Quaresimin M. Fatigue strength assessment of a short fiber composite based on the specific heat dissipation. Compos Part B-Eng 2011;42:217–25.
[9] Boulanger T, Chrysochoos A, Mabru C, Galtier A. Calorimetric analysis of dissipative and thermoelastic effects associated with the fatigue behavior of steels. Int J Fatigue 2004;26:221–9.
[10] Morabito AE, Chrysochoos A, Dattoma V, Galietti U. Analysis of heat sources accompanying the fatigue of 2024 T3 aluminium alloys. Int J Fatigue 2007;29:977–84.
[11] Chrysochoos A, Louche H. An infrared image processing to analyse the calorific effects accompanying strain localisation. Int J Eng Sci 2000;38:1759–88.
[12] Maquin F, Pierron F. Heat dissipation measurements in low stress cyclic loading of metallic materials: from internal friction to micro-plasticity. Mech Mater 2009;41:928–42.
[13] Connesson N, Maquin F, Pierron F. Experimental energy balance during the first cycles of cyclically loaded specimens under the conventional yield stress. Exp Mech 2010;51:23–44.
[14] Connesson N, Maquin F, Pierron F. Dissipated energy measurements as a marker of microstructural evolution: 316L and DP600. Acta Mater 2011;59:4100–15.
[15] Yang B, Liaw PK, Wang H, Jiang L, Huang JY, Kuo RC, et al. Thermographic investigation of the fatigue behavior of reactor pressure vessel steels. Mater Sci Eng, A 2001;314:131–9.
[16] Yang B, Liaw PK, Morrison M, Liu CT, Buchanan RA, Huang JY, et al. Temperature evolution during fatigue damage. Intermetallics 2005;13:419–28.
[17] Balandraud X, Le Cam JB. Some specific features and consequences of the thermal response of rubber under cyclic mechanical loading. Arch Appl Mech 2014;84:773–88.
[18] Wang XG, Crupi V, Guo XL, Zhao YG. Quantitative thermographic methodology for fatigue assessment and stress measurement. Int J Fatigue 2010;32:1970–6.
[19] Fan JL, Guo XL, Wu CW. A new application of the infrared thermography for fatigue evaluation and damage assessment. Int J Fatigue 2012;44:1–7.
[20] Germain P, Nguyen QS, Suquet P. Continuum thermodynamics. J Appl Mech 1983;50:1010–20.

[21] Coleman BD, Gurtin ME. Thermodynamics with internal state variables. J Chem Phys 1967;47:597–613.
[22] Amiri M, Khonsari MM. On the role of entropy generation in processes involving fatigue. Entropy 2011;14:24–31.
[23] Liakat M, Khonsari MM. Rapid estimation of fatigue entropy and toughness in metals. Mater Des 2014;62:149–57.
[24] Liakat M, Khonsari MM. Entropic characterization of metal fatigue with stress concentration. Int J Fatigue 2015;70:223–34.
[25] Fan GD, Zheng MY, Hu XS, Xu C, Wu K, Golovin IS. Improved mechanical property and internal friction of pure Mg processed by ECAP. Mater Sci Eng, A 2012;556:588–94.
[26] Fan GD, Zheng MY, Hu XS, Xu C, Wu K, Golovin IS. Effect of heat treatment on internal friction in ECAP processed commercial pure Mg. J Alloys Compd 2013;549:38–45.
[27] Mareau C, Favier V, Weber B, Galtier A, Berveiller M. Micromechanical modeling of the interactions between the microstructure and the dissipative deformation mechanisms in steels under cyclic loading. Int J Plast 2012;32–33:106–20.
[28] Mareau C, Cuillerier D, Morel F. Experimental and numerical study of the evolution of stored and dissipated energies in a medium carbon steel under cyclic loading. Mech Mater 2013;60:93–106.
[29] Cura F, Curti G, Sesana R. A new iteration method for the thermographic determination of fatigue limit in steels. Int J Fatigue 2005;27:453–9.
[30] Risitano A, Risitano G. Cumulative damage evaluation in multiple cycle fatigue tests taking into account energy parameters. Int J Fatigue 2013;48:214–22.
[31] Risitano A, Risitano G. Cumulative damage evaluation of steel using infrared thermography. Theor Appl Fract Mech 2010;54:82–90.
[32] Montgomery DC, Runger GC, Hubele NF. Engineering statistics. John Wiley & Sons; 2009.
[33] Hogg RV, McKean J, Craig AT. Introduction to mathematical statistics. Pearson Education; 2005.
[34] Granato A, Lucke K. Application of dislocation theory to internal friction phenomena at high frequencies. J Appl Phys 1956;27:789–805.
[35] Granato A, Lucke K. Theory of mechanical damping due to dislocations. J Appl Phys 1956;27:583–93.
[36] Frank F, Read W. Multiplication processes for slow moving dislocations. Phys Rev 1950;79:722–3.
[37] Burton WK, Cabrera N, Frank FC. The growth of crystals and the equilibrium structure of their surfaces. Philos Trans R Soc A 1951;243:299–358.